

## Degradation behaviors and in-vivo biocompatibility of a rare earth- and aluminum-free magnesium-based stent

Bian, Dong; Zhou, Xiaochen; Liu, Jianing; Li, Wenting; Shen, Danni; Zheng, Yufeng; Gu, Wenda; Jiang, Jingjun; Li, Mei; Chu, Xiao

**DOI**

[10.1016/j.actbio.2021.01.031](https://doi.org/10.1016/j.actbio.2021.01.031)

**Publication date**

2021

**Document Version**

Final published version

**Published in**

Acta Biomaterialia

**Citation (APA)**

Bian, D., Zhou, X., Liu, J., Li, W., Shen, D., Zheng, Y., Gu, W., Jiang, J., Li, M., Chu, X., Ma, L., Wang, X., Zhang, Y., Leeflang, S., & Zhou, J. (2021). Degradation behaviors and in-vivo biocompatibility of a rare earth- and aluminum-free magnesium-based stent. *Acta Biomaterialia*, 124, 382-397. <https://doi.org/10.1016/j.actbio.2021.01.031>

**Important note**

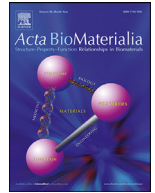
To cite this publication, please use the final published version (if applicable). Please check the document version above.

**Copyright**

Other than for strictly personal use, it is not permitted to download, forward or distribute the text or part of it, without the consent of the author(s) and/or copyright holder(s), unless the work is under an open content license such as Creative Commons.

**Takedown policy**

Please contact us and provide details if you believe this document breaches copyrights. We will remove access to the work immediately and investigate your claim.



## Full length article

## Degradation behaviors and *in-vivo* biocompatibility of a rare earth- and aluminum-free magnesium-based stent



Dong Bian<sup>a</sup>, Xiaochen Zhou<sup>b</sup>, Jianing Liu<sup>c</sup>, Wenting Li<sup>b</sup>, Danni Shen<sup>b</sup>, Yufeng Zheng<sup>a,b,c,\*</sup>, Wenda Gu<sup>d</sup>, Jingjun Jiang<sup>e,\*</sup>, Mei Li<sup>a</sup>, Xiao Chu<sup>a</sup>, Limin Ma<sup>a</sup>, Xiaolan Wang<sup>a</sup>, Yu Zhang<sup>a</sup>, Sander Leeflang<sup>f</sup>, Jie Zhou<sup>f,\*</sup>

<sup>a</sup> Department of Orthopedics, Guangdong Provincial People's Hospital, Guangdong Academy of Medical Sciences, Guangzhou, 510080, China

<sup>b</sup> Department of Materials Science and Engineering, College of Engineering, Peking University, Beijing, 100871, China

<sup>c</sup> Academy for Advanced Interdisciplinary Studies, Peking University, Beijing, 100871, China

<sup>d</sup> Department of Cardiac Surgery, Guangdong Provincial People's Hospital, Guangdong Academy of Medical Sciences, Guangzhou, 510080, China

<sup>e</sup> Department of Vascular Surgery, Peking University People's Hospital, Beijing, 100044, China

<sup>f</sup> Department of Biomechanical Engineering, Delft University of Technology, Mekelweg 2, 2628 CD Delft, Netherlands

## ARTICLE INFO

## Article history:

Received 29 September 2020

Revised 14 January 2021

Accepted 19 January 2021

Available online 27 January 2021

## Keywords:

Biodegradable stent

Mg-Li alloy

Degradation behavior

Biocompatibility

Iliac artery

## ABSTRACT

Biodegradable stents can provide scaffolding and anti-restenosis benefits in the short term and then gradually disappear over time to free the vessel, among which the Mg-based biodegradable metal stents have been prosperously developed. In the present study, a Mg-8.5Li (wt.%) alloy (RE- and Al-free) with high ductility (> 40%) was processed into mini-tubes, and further fabricated into finished stent through laser cutting and electropolishing. *In-vitro* degradation test was performed to evaluate the durability of this stent before and after balloon dilation. The influence of plastic deformation and residual stress (derived from the dilation process) on the degradation was checked with the assistance of finite element analysis. In addition, *in-vivo* degradation behaviors and biocompatibility of the stent were evaluated by performing implantation in iliac artery of minipigs. The balloon dilation process did not lead to deteriorated degradation, and this stent exhibited a decent degradation rate (0.15 mm/y) *in vitro*, but divergent result (> 0.6 mm/y) was found *in vivo*. The stent was almost completely degraded in 3 months, revealing an insufficient scaffolding time. Meanwhile, it did not induce possible thrombus, and it was tolerable by surrounding tissues in pigs. Besides, endothelial coverage in 1 month was achieved even under the severe degradation condition. In the end, the feasibility of this stent for treatment of benign vascular stenosis was generally discussed, and perspectives on future improvement of Mg-Li-based stents were proposed.

## Statement of significance

In the present study, a Mg-8.5Li (wt.%) alloy (RE- and Al-free) with a good ductility was processed into finished stents. *In-vitro* degradation behaviors of the stent before and after balloon dilation were comparatively studied, with the assistance of finite element analysis. *In-vivo* degradation behaviors and biocompatibility of the stent were evaluated by performing implantation in iliac artery of minipigs. The stent exhibited a decent degradation rate (0.15 mm/y) *in vitro*, but divergent result (> 0.6 mm/y) was found *in vivo*. The stent did not induce possible thrombus, and it was tolerable by surrounding tissues. Moreover, endothelial coverage in 1 month was achieved. Apparently, Mg-Li based biodegradable stent shows virtue from the criteria of elemental biocompatibility.

© 2021 Acta Materialia Inc. Published by Elsevier Ltd. All rights reserved.

## 1. Introduction

Since the first implantation of a coronary artery stent (bare metallic stent) in 1986 [1,2], stent has become a dominant medical apparatus in the treatment of vascular stenosis [3,4]. Up to now,

\* Corresponding authors.

E-mail address: [yfzheng@pku.edu.cn](mailto:yfzheng@pku.edu.cn) (Y. Zheng).

the stent has experienced mainly three generations of innovation: bare metallic stent (BMS), drug-eluting stent (DES) and biodegradable stent (BDS) [5–7]. The restenosis rate has been well controlled (< 5%) with current DESs [8,9]. Nonetheless, complications such as risks of late stent thrombosis and impaired endothelial function still remained a concern as the lifelong existing of DES [10–14]. There are few reasons for the permanent remaining of the stent when remodeling of the stented vessel is completed [15]. Spontaneously, BDS seems to be the next generation and the ideal stent in the treatment of vascular stenosis.

Lately, magnesium-based (Mg-based) stents have attracted great attention as a revolutionized generation of BDS [6],[16]. In 2016, the Mg-based drug-eluting stent Magmaris (BIOTRONIK, Germany) received the CE mark approval [17,18]. This new type of metallic BDS is expected to provide a temporary opening to a narrowed arterial vessel until the vessel remodeling is done, and to disappear progressively thereafter [19]. It opens a new horizon in the development of metallic BDSs, and also in the treatment of narrowed vessels. The promising results with good clinical and safety outcomes up to 3 years' follow-up support the use of Magmaris in simple coronary artery disease [20].

Owing to the unique biodegradability and good biocompatibility of Mg [21,22], concerns with traditional BMSs or DESs, such as late thrombosis, long-term endothelial dysfunction, permanent physical irritation, chronic inflammatory local reactions, restricted vasoreactivity, etc., could possibly be avoided in Mg-based BDSs. Blood vessels are set free from the metallic cage after full degradation of Mg-based BDSs [23]. This is particularly important in pediatrics as blood vessels of children and adolescents are immature, and they continue to grow. In addition, full degradation makes the re-stenting possible, and it also ameliorates the vessel wall quality. Due to the metallic nature, mechanical properties (radial strength, deformability, deliverability, etc.) of Mg-based BDSs are superior to their polymeric competitors. The body's ability to quickly resorb Mg leads to a faster and therefore more desirable resorption time than the polymer-based BDSs. Mg-based BDSs could emerge as a strong alternative to currently available polymeric BDSs.

In the past decades, some magnesium alloys have been developed as potential BDS materials, but only limited ones were fabricated into stents and performed animal trials, which include WE43 [24], AE21 [25], AZ31B [26], AZ91 [27], Mg-Nd-Zn-Zr [28], etc. Among them, only the WE43-based one entered the clinical trial and finally received CE mark approval [20]. The vast majority of those alloys were aluminum (Al) containing or rare earth (RE) containing alloys. However, Al in biomedical applications is discouraged because of its possible toxicity [29]. Rare earth elements are not essential to human, and the long-term effect of RE on blood vessels needs further research [30,31]. From the perspective of biological safety, the ideal alloying elements in Mg-based BDSs should be those which are essential to or naturally presented in human body [16].

Lithium (Li) is naturally presented in human body, and it is a possibly essential element to human health (still a controversial issue) [32,33]. Lithium salts have been used in the treatment of bipolar disorder for a long time at a proper dosage range (oral intake of 113–226 mg Li per day) [16,32,34,35]. Bosche et al. [36] found that low-dose lithium could act as a drug directly stabilizing human endothelium and ubiquitously augmenting cholinergic endothelium-mediated vasorelaxation. It is one of the two known elements (the other one is rare earth element scandium) which can change the hexagonal close-packed structure (hcp) of magnesium into body-centered cubic type (bcc), in this way improving ductility [37]. Just in time, good deformability is crucial for balloon expandable stent. So, Li is a proper alloying element for magnesium alloys developed for BDSs. The good biocompatibility of Mg-Li based alloys have already been proved in bones [38],[39].

However, no intravascular implantation of the Mg-Li alloy system has been reported yet.

In our previous study [40],[41], a Mg-8.5Li (wt.%) alloy composed of duplex  $\alpha+\beta$  phases was found to exhibit a high ductility (elongation > 40%), and this was particularly attractive for radially expandable stent applications. Cytotoxicity tests confirmed that the Mg-8.5Li alloy was compatible with human umbilical vein endothelial cells (ECV304), while it significantly inhibited the proliferation of rodent vascular smooth muscle cells (VSMC) with increasing culture time. This property might be favorable for promoting endothelialization and inhibiting excessive VSMC hyperplasia. In addition, this alloy showed proper hemocompatibility (hemolysis ratio < 5%, no activation of platelets, with normal coagulation parameters *in vitro*).

Based on the previous results, the Mg-8.5Li alloy was processed into mini-tube, and further fabricated into finished stent through laser cutting, acid pickling and electropolishing, respectively. The structural integrity of the Mg-8.5Li stent after balloon dilation was simulated through finite element analysis (FEA), and was also verified through experimental observation. The *in-vitro* degradation behaviors before and after balloon dilation were compared. Furthermore, the stent was deployed into iliac artery in minipigs, and *in-vivo* performances were evaluated through micro-CT scanning and histopathological examination. The feasibility of this stent to be used in stenosed vessels was generally discussed. In the end, outlooks on the future development of Mg-Li alloy based BDSs were proposed.

## 2. Material and methods

### 2.1. Preparation of Mg-Li mini-tube and stent fabrication

The preparation of Mg-Li mini-tubes was performed in Delft University of Technology. A binary Mg-8.5Li alloy was supplied in as-cast form and was machined into extrusion billets with a diameter of 48 mm and a length of 200 mm. The Li content of the Mg-8.5Li billets, determined by using inductively coupled plasma optical emission spectrometry (ICP-OES, Prodigy 7, Leeman), was 8.48 wt.%. Those billets were preheated at 250 °C for 1 h, and then extruded at a reduction ratio of 20 and at a ram speed of 1 mm/s into bars with a diameter of 11.2 mm by using a 250 MT direct extrusion press. The extruded bars were machined into hollow billets with an outside diameter (OD) of 11 mm and a length of 26 mm. Then, they were indirectly extruded at 250 °C into mini-tubes with an OD of 3.2 mm, an insider diameter (ID) of 2.5 mm. Mg-Li stents were directly laser cut from those mini-tubes, and followed by acid pickling and electropolishing in Jiangyin Fasten-PLT Materials Science Co. Ltd. Some auxiliary accessories were used to keep the Mg tube straight during laser cutting. Burrs after laser cutting were removed through acid pickling. The weight and strut dimensions of the finished stent were guaranteed through control of the material removal amount during electropolishing. This stent exhibits a low elastic recoil ( $1.72 \pm 0.31\%$ , radial) and a limited amount of foreshortening ( $3.20 \pm 1.75\%$ , axial), with a radial strength of  $59.5 \pm 4.6$  kPa. Pattern design of the stent was illustrated in Fig. 1(a). The stent for animal test was pre-mounted on a self-designed delivery balloon-catheter system, individually encapsulated, and sterilized under Co60 radiation before use.

### 2.2. Finite element analysis (FEA) of the stent

All the material parameters of the stent were obtained through experimental measurement. Fig. 1(c) displays the true stress-strain curve of the extruded Mg-8.5Li alloy. A homogeneous, isotropic, elasto-plastic material model was used. The 2D geometry model of the stent was created in SolidWorks 2014, as shown in Fig. 1(a).

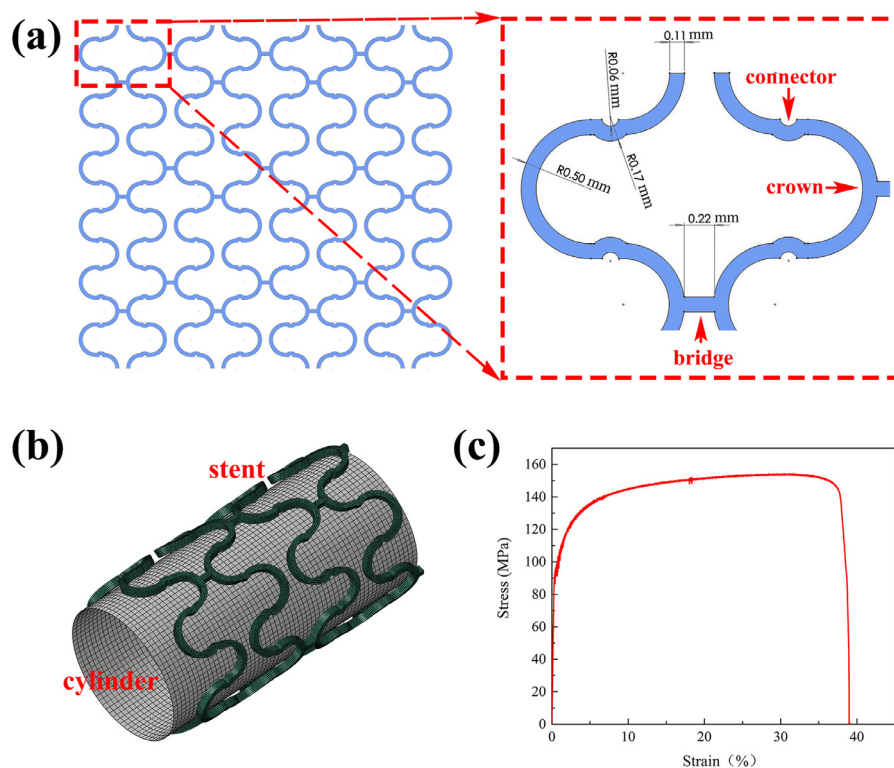


**Fig. 1.** (a) Schematic pattern design of the Mg-8.5Li stent, with typical regions and dimension parameters shown in the enlarged image, (b) the FEA model composed of a stent and one cylinder, (c) typical tensile curve of the Mg-8.5Li alloy.

Then it was imported into Pro/E 5.0 to form the 3D model. The mesh generation was carried out in HyperMesh 12.0. The mesh density was studied, and a proper mesh density was used in all the simulations in this work. Abaqus 2016 was used to run the simulations. The FEA model was composed of two parts, i.e. a Mg-8.5Li stent and one cylinder, as depicted in Fig. 1(b). The length of the cylinder is slightly longer than that of the stent. After the stent was dilated/expanded to a certain size by means of expanding the inner cylinder, it recoiled after removing the cylinder. The mirror symmetry along the generatrix allows to simulate only half of the stent in order to reduce the model size. A static analysis was performed with nonlinear geometry option to better simulate the dilation and recoil processes. All the contact frictions were ignored in the analysis for simplicity.

In these simulations, cylindrical coordinates were used. A cylinder was introduced to control the dilation and recoil processes. The stent with the element type of C3D8R and the cylinder with the element type of SFM3D4R were coaxial. For the half stent, the axial degree of freedom was fixed at the open ends, and the circumferential degree of freedom was fixed at one node to prevent the rigid body rotation. For the cylinder, both circumferential and axial degrees of freedom are fixed. A radial displacement was applied to the nodes of the cylinder to increase the inner radius to 1.75 mm. Then, a  $-0.35$  mm radial displacement was applied to the nodes of the cylinder to let the stent gradually recoil. The stress and strain distributions on the stent during dilation and recoil were analyzed.

### 2.3. In-vitro degradation characterization

Eight stents were used for *in-vitro* degradation test, and four of them were balloon dilated by using a balloon-catheter system ( $\Phi 3.5 \times 20$  mm, Boston Scientific) at the nominal pressure (NP, 8 atm) for 30 s. The surface integrity of the dilated stent was examined under a scanning electron microscope (SEM, HITACHI S-4800,

Japan), equipped with an energy dispersive spectrometer (EDS). Static immersion test was carried out in Hank's solution (H1025, Solarbio) at  $37 \pm 0.5$  °C with an exposure ratio of 20 mL/cm<sup>2</sup>, according to ASTM-G31-72 [42]. Every stent was placed into an individual centrifuge tube (15 mL, Corning), which was incubated in a  $37 \pm 0.5$  °C water bath. During immersion, pH value of the Hank's solution was monitored by using a pH meter (PB-10, Sartorius), with normal Hank's solution as control. Concentrations of Mg, Li, Ca and P in the solution after immersion were measured by ICP-OES (iCAP 6000, Thermo). The macro-morphology of the stent after immersion was captured under a digital camera (Canon EOS 70D, Japan). The surface was characterized by a Fourier transform infrared spectrometer (FTIR, Nicolet iS 50, Thermo Scientific) and an imaging X-ray photoelectron spectrometer (XPS, Axis Ultra, Kratos Analytical Ltd.). The FTIR spectrum was recorded over a range of 4000–500 cm<sup>-1</sup> to identify functional groups in the sample surface. High resolution narrow scanning of XPS was performed to determine the binding states of Mg 2p, O 1 s, Ca 2p, P 2p, C 1 s, and Na 1 s, by using Al K $\alpha$  radiation. Constituent phases in the degradation product layer were identified by using an X-ray diffractometer (XRD, X'Pert Pro-MPD). Considering the small and irregular testing area on the stent, XRD test was performed by using a Mono-Capillary PreFix Module operating at 45 kV and 40 mA with Cu K $\alpha$  radiation, at a step size of 0.017° over a range of 10–90°. The structural integrity of stents was examined under a micro-CT scanner (Latheta LCT 200, Hitachi-Aloka) at a spatial resolution of 24  $\mu$ m. The 3D reconstruction was performed in Amira software (Amira 6.0.1, Visage Imaging). One unexpanded stent along with an expanded stent was embedded in cold mounting resin (BUBBLEFREE, TRUER) for cross-section analysis. Samples were also observed under SEM before and after removing the degradation products in chromic acid (200 g CrO<sub>3</sub> in 1000 mL H<sub>2</sub>O), according to ASTM G1-03(2017) e1 [43]. The degradation rate was calculated according to the following equation,  $CR = 3.65\Delta W/\rho$  [44], where

$\Delta W$  is the metal weight loss rate ( $\text{mg}/\text{cm}^2/\text{d}$ ) and  $\rho$  is the metal density ( $\text{g}/\text{cm}^3$ ).

## 2.4. In-vivo degradation and biocompatibility

### 2.4.1. Animal model and surgery

Porcine artery is a proper and commonly used model for *in-vivo* stent evaluations (embolism, thrombosis, local tissue responses, etc.) [45]. Animals were supplied by Beijing Ke Xing Experimental Animal Cultivation Center (animal use permit No.: SCXK (jing) 2012–0005). Six laboratory minipigs were fed with aspirin 3 days before operation at a dosage of 100 mg/d. The surgery was performed under general anesthesia by intravenous injection of 2% pentobarbital at the dosage of 30 mg/kg. Animals were placed abdomen-up and limbs fixed. Bilateral iliac arteries were isolated after opening the abdomen. Lumen diameter was measured through ultrasonography (GE Logic E), and it was in the range of 3.0–3.3 mm. A sheath (6Fr, TERUMO) was punched into the artery along the blood descending direction. After administration of unfractionated heparin through peripheral vein (systemic anticoagulation, 1 mg/kg), a Mg-8.5Li stent was delivered into the iliac artery (either left or right) and balloon dilated at 8 atm (NP, a nominal diameter of 3.5 mm) for 30 s to deploy the stent, under the guidance of a guide wire (0.014 inch). The contralateral iliac artery without implantation was set as normal control. Position of the stent was marked by two stitches at the adjacent tissues on both ends of the stented section (a total marked vessel length of 5 cm), in much convenience for recycling samples. The artery patency was confirmed by intraoperative ultrasonography. Finally, the wound was well sutured (7–0 Prolene) and patched with aseptic dressing. Antiplatelet therapy was performed by giving 100 mg aspirin daily after the implantation. Two animals were sacrificed at 1, 2 and 3 months post-operation, respectively. The patency of the iliac artery was confirmed through ultrasonography during the dissection. The stented iliac artery and the normal iliac artery were both retrieved for follow-up analysis. The anesthetic, surgical and post-operative care protocols were examined by and fulfilled the requirements of the Ethics Committee of Peking University People's Hospital (Animal Trial Permit No. 2014–29, the Ethics Committee of Peking University People's Hospital).

### 2.4.2. In-vivo degradation and histological evaluation

Retrieved iliac arteries were immediately examined under a micro-CT scanner (Skyscan1076, Bruker) at a spatial resolution of 9  $\mu\text{m}$ . The 3D reconstruction of the remaining stent was performed in Mimics software (Mimics 10.01, materialise Mimics®). Pathological examination of the stented vessel and the normal vessel was performed by using conventional paraffin-embedded sectioning and staining with hematoxylin-eosin (H&E, Guge Biological Technology Co., Ltd.). Specifically, one sample at 1 month was longitudinally cut open and separated into two parts. One part was fixed in 2.5% glutaraldehyde solutions followed by dehydration in gradient ethanol/distilled water mixtures (50%, 60%, 70%, 80%, 90% and 100%, 10 min for each). The endothelialization condition of the stent was observed under SEM after spraying with Au. For the other part, the remaining stent was directly extracted from the vessel tissues and examined under SEM.

## 2.5. Statistical analysis

Data in this work were expressed as means  $\pm$  standard deviation. Statistical analysis was performed with SPSS 18.0 software (SPSS Inc., Chicago, USA). Differences between groups were analyzed by using one-way analysis of variance (ANOVA) followed by Tukey test. The statistical significance was defined as  $p < 0.05$ .

## 3. Results

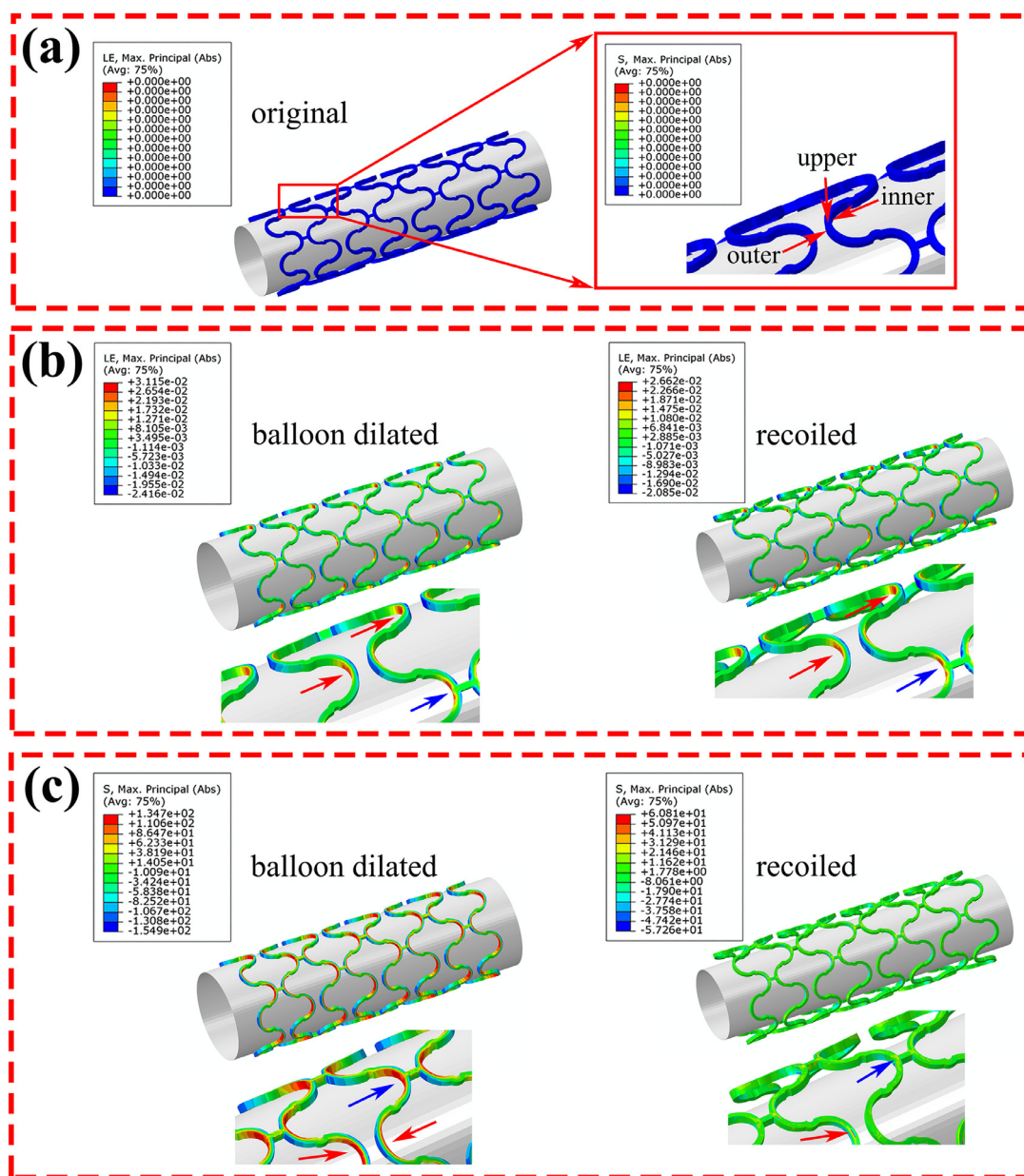
### 3.1. FEA result

Fig. 2 shows the distribution of principal strain and stress on the stent after it was dilated and naturally recoiled. The maximum principal strain after dilation was mainly concentrated at the crown (typical position of each part on the stent is indicated in Fig. 1(a)), with tension strain at the inner surface and compression strain at the other side, i.e. the outer surface of the crown. The maximum principal strain after dilation (similar to balloon dilation to 3.5 mm) was 3.12% (7.8% of the total elongation), which was well below the fracture limit of Mg-8.5Li alloy ( $> 40\%$ ). The bridge between two crowns alleviated the principal strains at both neighboring crowns, as indicated by blue arrows in Fig. 2(b) (compared with the red arrow indicated sites). The distribution of the maximum principal stress during dilation was similar to that of the maximum principal strain, all concentrated at the crowns, as marked by red arrows in Fig. 2(c). A maximum principal stress (tension) of 134.7 MPa (87.5% of the ultimate tensile strength) and a radial recoil of 3.3% (a little higher than the actual test value) were found after dilation and deflation, respectively. The distribution of residual stress after unloading was presented in the right side of Fig. 2(c). A maximum residual tension stress of 60.8 MPa (39.5% of the ultimate tensile strength) appeared near the outside surface of the crown (upper site, the orientation is illustrated in Fig. 2(a)) while the maximum residual compression stress was found near the internal surface at the crown, as shown in the enlarged images. Generally, the balloon dilation process would not induce any damage to the stent, judging from the FEA results.

### 3.2. In-vitro degradation behavior

Fig. 3 shows the macroscopic morphologies of the stent before and after immersion under an optical camera and under radioscopy. The original stent owned a smooth surface and was shining with metallic luster. Balloon dilation (8 atm, expansion to  $\Phi 3.5$  mm) did not induce any visible fractures or defects on the stent (inspection under an optical microscope and under SEM at high magnifications). The dogboning effect during dilation was not obvious. The deformation of Mg-8.5Li stent was generally uniform in both axial and radial directions. After immersion for 7 days, the stent surface became pale, and a greyish degradation product layer could be observed. A fracture occurred casually at a strut section on one of the unexpanded stents, as indicated by red arrows in Fig. 3(a). The stent integrity after immersion was examined under X-ray, as depicted in Fig. 3(b). Generally, the structural integrity was mainly maintained after immersion. However, at limited sites, low-density areas were found under X-ray, showing the appearance of localized degradation. At those sites, the remaining stent struts became much thinner, as revealed by the micro-CT results. The localized degradation was suspected to be closely related to the componential (impurities) and microstructural heterogeneity.

Fig. 4 shows the microscopic morphologies of the stent before and after removing the degradation products. Surface details could be revealed under SEM. Before immersion, the original stent exhibited a smooth surface without sharp edges. After balloon dilation, the stent surface kept intact without any fractures/cracks, indicating the good deformability. After immersion, the strut surface was covered with a degradation product layer with some white deposits on top of it. This layer was mainly composed of Mg, O, Ca, P, C and Na, as revealed by EDS analysis. Degradation of the stent was generally uniform. However, a few localized degradation sites were also found on the stents whether they were dilated or not, as marked by red arrows. Degradation products accumulated on those sites and they were in a loose condition. The



**Fig. 2.** (a) Typical positions on the stent as indicated by red arrows, (b) the distribution of principal strain on the stent during balloon dilation and natural recoil, red arrows showing the sites with maximum principal strain, blue arrows showing alleviated principal strain at connected neighboring crowns, (c) the distribution of principal stress on the stent during balloon dilation and natural recoil, with red arrows showing the sites with maximum principal stress (tension), blue arrows showing alleviated principal stress at connected neighboring crowns. (For interpretation of the references to colour in this figure legend, the reader is referred to the web version of this article.)

sites where localized degradation happened seemed to be irregular and random, not appearing at a specific site. After removing the degradation products, the actual morphology of the strut was exposed. Except for the limited local degradation sites, the stent exhibited a generally uniform degradation morphology. At severely localized degradation sites, deep holes were revealed. The degradation seemed to be preferentially occurred at specific directions, maybe along specific lattice planes, as revealed in the inserts in Fig. 4(b). On the microscopic level, the stent is susceptible to pitting, as shown in the enlarged SEM images. Clear and intact grain boundaries could still be observed after removing the degradation products, as shown in inserts of Fig. 4(b). The degradation at the grain boundaries was not severe than the degradation in the interior of the grains, suggesting that grain boundaries were not the vulnerable sites during degradation.

Fig. 5(a) displays the cross-sectional morphologies of the stents and corresponding EDS element mapping (red: Mg, green: O, blue: Ca, cyan: P, purple: C). The stent strut was covered by a thin degradation product layer. In areas where degradation was more severe, this layer was much thicker. Ca and P were found to be enriched in the surface of the degradation products, indicating Ca/P deposits on the degradation product layer.

Fig. 5(b) and (c) shows the pH variation during a 7-day-immersion and element concentrations after immersion, respectively. At the beginning, there was a certain pH increase of the Hank's solution, suggesting a fast stent degradation during this period. Afterwards, the pH value increased slowly and finally reached a relatively stable value around 8.8 in the experimental groups. During the whole immersion period, pH value of the dilated stent group was always slightly higher than that of the unexpanded

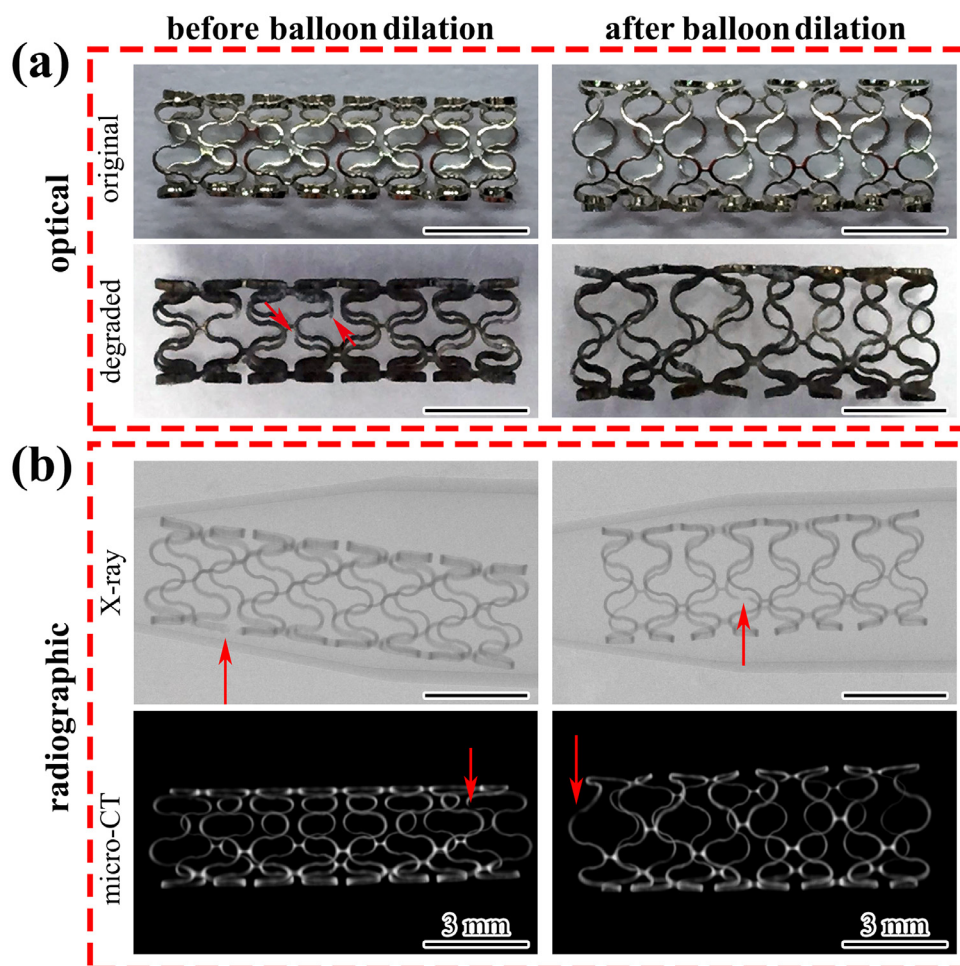


**Fig. 3.** (a) Macroscopic morphologies of the stent (either dilated or not) before and after immersion in Hank's solution for 7 days under an optical camera, (b) macroscopic morphologies of the stent (either dilated or not) after immersion in Hank's solution for 7 days under a micro-CT scanner, with red arrows indicating the localized degradation sites. (For interpretation of the references to colour in this figure legend, the reader is referred to the web version of this article.)

group (stent without dilation). However, there was no significant difference. There was almost no difference in the Mg and Li concentrations between those two groups, as shown in Fig. 5(c). Compared to the blank control group, reduced Ca and P were detected after immersion in the experimental groups with Mg-8.5Li stents. Deposition of Ca and P on the degraded stent should be responsible for their decrease in the medium. Degradation rates (calculated from weight loss) of the stents before dilation and after dilation were  $0.113 \pm 0.028$  mm/y and  $0.145 \pm 0.031$  mm/y, respectively. A little higher degradation rate was found in the balloon dilated group. However, no significant difference was detected.

Fig. 6 shows the XPS, FTIR and XRD results of the Mg-8.5Li stent after immersion. XPS result revealed that elements including Mg, O, Ca, P, C and minor Na were detected on the sample surface. High resolution narrow scanning confirmed the possible presence of calcium phosphate or hydroxyapatite on the surface, as indicated by the Ca 2p peak at 350.90 eV, along with P 2p peak at 133.36 eV and O 1 s peak at 531.17 eV [46,47]. The O 1 s peak at 532.65 eV and C 1 s peak at 284.87 eV could be attributed to the  $\text{CO}_3^{2-}$  [46]. The Na 1 s peak at 1071.82 eV is assigned to a small amount of NaCl, which precipitated from the Hank's solution. FTIR spectrum indicated the presence of possible functional groups including  $\text{H}_2\text{O}$ ,  $\text{OH}^-$ ,  $\text{CO}_3^-$ ,  $\text{PO}_4^{3-}$  and possible  $\text{H}_2\text{PO}_4^{2-}$  [48,49], as shown in Fig. 6(b). The mainly crystalline degradation products could be directly identified through XRD analysis, and they were mainly composed of  $\text{Mg}(\text{OH})_2$ ,  $\text{MgCO}_3 \cdot 2\text{H}_2\text{O}$  and  $\text{CaMg}_5(\text{CO}_3)(\text{PO}_4)_4(\text{OH})$ , as

depicted in Fig. 6(c). Weak peaks from the  $\beta$ -Li phase could also be detected through XRD analysis.

### 3.3. In-vivo degradation and biocompatibility

Fig. 7(a) shows the stent implantation process and retrieval of the target vessels. After the laparotomy, patency of the stented vessels was verified through ultrasonic examination, and all the implanted vessels showed unobstructed blood flow. There was no noticeable difference between the stented vessels and the normal control vessels through gross examination. The stent could be felt through gentle touch along the stented vessels after 1 month. In the next month, the stent could be barely felt, implying serious degradation by this time (2-month post-operation). The stented vessels exhibited good vascular adaptability as they could be easily curled and twisted without sensation of foreign matter at month 3. No thrombosis or blood clotting was found in the stented section or far from the stent through general observation.

Fig. 7(b) displays the 3D reconstruction of the remaining stent in the iliac arteries. The major part of the stent still existed, and the remaining stent kept as a whole after 1 month. Even though some struts fractured, the structure and shape of the stent could still be distinguished. The remaining part maintained most of its structural integrity. After 2 months, the stent was seriously degraded as the remaining part has fractured into small pieces, and the stent units were no longer interconnected. The stent strut

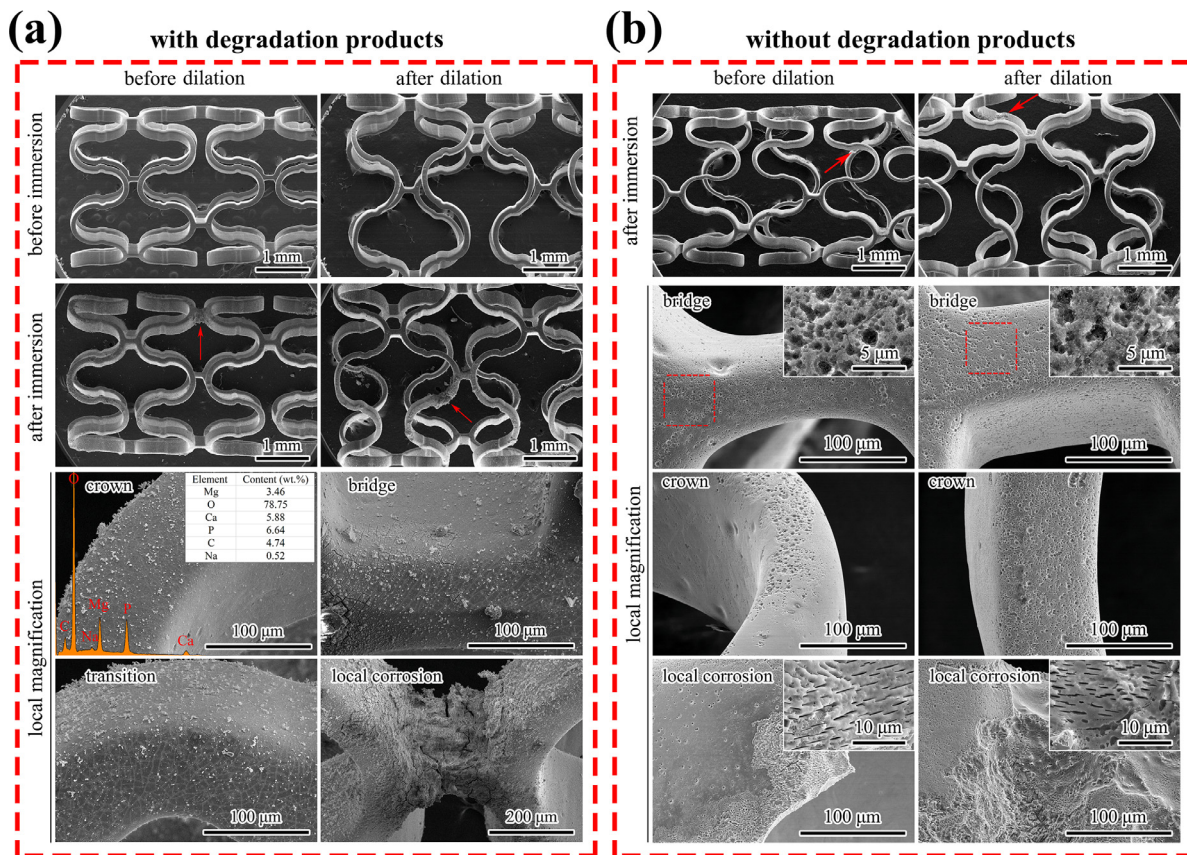


**Fig. 4.** (a) Microscopic morphologies of the stent (either dilated or not) before and after immersion in Hank's solution for 7 days under SEM, (b) Microscopic morphologies of the degraded stent after removing the degradation products under SEM, with enlargement of typical areas.

has become much thinner and rougher compared to that at 1 month. After 3 months, only some residual particles in limited size and limited amount could be detected. No substances with density higher than the vessel wall could be found in the normal control vessels. Generally, the Mg-8.5Li stent exhibited an over-quick degradation *in vivo*, and it was almost fully degraded after 3 months (*in-vivo* degradation rate > 0.6 mm/y).

Histological images of the stented iliac arteries at different time points were listed in Fig. 7(c), with normal iliac artery as control. The voids where the stent struts previously occupied before slicing and staining could be clearly seen, as indicated by black triangles. Endothelial coverage in the first month could be found as the struts were covered by a monolayer of cells. Due to the mechanical mismatch between the stent platform and paraffin permeated tissues, some of the tissues were torn away from their original positions during slicing procedure, as indicated by the long red arrow in Fig. 7(c). Only limited stent remnants were observed after 2 months, and the surrounding tissues penetrated into the spaces where the stent struts held before. At month 2, the stent struts were embedded in the middle layer of the vascular membrane, well beneath the intima. A certain degree of inflammatory response was observed. The adjacent tissues surrounding the struts appeared to be a little bit loose and irregular at month 2, when compared to the normal control or tissues at month 3. It was probably caused by the fast stent degradation and the by-products (hydrogen, degradation products) which were generated during stent degradation.

During stent degradation, some debris or degradation products could also be observed in the tissues adjacent to the stent struts, as illustrated by red arrows in Fig. 7(c). After implantation for 3 months, no obvious stent debris or residues could be found

through histological examination, implying that the Mg-8.5Li stent could be fully absorbed soon after. The tiny particles observed under micro-CT at month 3 (Fig. 7(b)) were not easily found in the histological images (Fig. 7(c)), since they were in limited size and were not easy to be exactly sliced. The recovered artery tissues at month 3 exhibited no microscopic difference to the normal iliac artery. However, unfortunately, the intima-medial thickness was thicker than the normal control.

Fig. 8(a) depicts the endothelial coverage status of the Mg-8.5Li stent after 1 month. The corresponding morphology of the stent after directly extracted from the vascular tissues was shown in Fig. 8(b). Endothelial cells could migrate across the protuberant struts, and then covered the whole stent. After 1 month, a monolayer of fusiform endothelial cells was formed on the stent struts, consistent with the histological results at 1 month. The endothelialization is favorable for lowering possible adverse reactions, such as restenosis and thrombus. As for the stent itself, a degradation product layer was formed. This layer was ruptured and peeled off due to dissociation (separation from the tissue) and dehydration. Elements of Mg, O, Ca, P, C, Na were detected in the degradation product layer through EDS characterization. In the peeling-off areas, such as area B, contents of Ca and P were less than those in the intact areas (area A). Meanwhile, higher contents of O and C were found in peeling-off areas. This suggested that Ca and P tended to be enriched on the surface of the degradation product layer. Similar results were also observed during the *in-vitro* degradation of Mg-8.5Li stent. Elements in the degradation products were similar both *in vitro* and *in vivo*, so as the XPS results. So, the major constituent phases in the degradation product layer should also be alike.

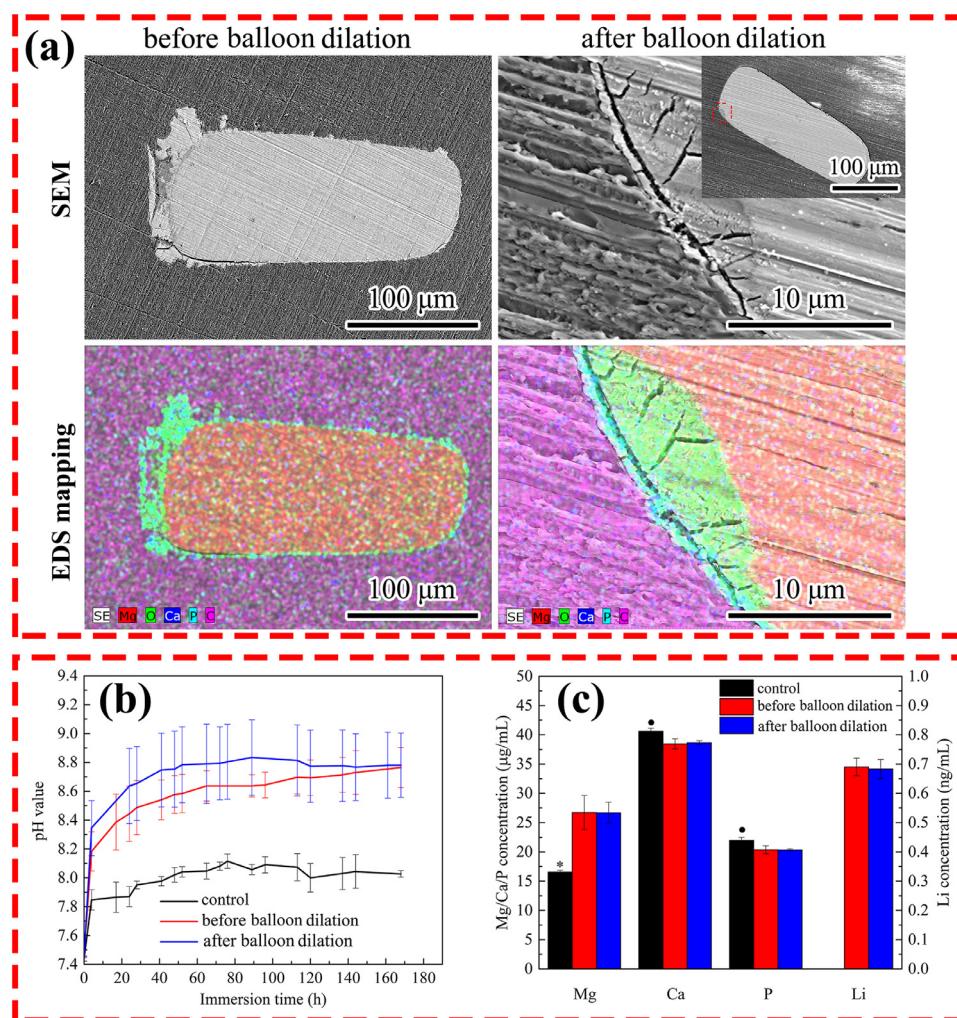


**Fig. 5.** (a) Cross-sectional morphologies of the degraded stents and corresponding EDS element mapping (red: Mg, green: O, blue: Ca, cyan: P, purple: C), (b) pH variation during a 7-day immersion in Hank's solution at 37 °C, (c) element concentrations (Mg, Li, Ca, P) in Hank's solution after immersion for 7 days, normal Hank's solution as control, \*  $p < 0.05$ , \*  $p < 0.01$ . (For interpretation of the references to colour in this figure legend, the reader is referred to the web version of this article.)

## 4. Discussion

### 4.1. The feasibility of Mg-8.5Li alloy stent for treatment of benign luminal diseases

Even though the addition of Li in our Mg-Li alloy is as much as 8.5 wt.%, the total Li content in the stent is still low, considering its limited size and weight. One Mg-8.5Li stent in present study weighs at 7 mg, and the total Li content accounts for 0.595 mg. This Li content will be gradually released in several months after implantation (a 3-month period in this study). The total Li content and the Li release per day (an average release rate of several micrograms) are both in the range of daily Li intake (several to several thousand micrograms per day), and far less than its therapeutic dose (113–226 mg of elemental lithium) or toxic dose [32,50]. This Li concentration in the stent is assumed to be acceptable.

One of the most crucial problems for Mg-based BDSs is that they degraded too fast, and premature loss of radial force before vascular remodeling might lead to restenosis. Erinc et al. [51] proposed that degradation rate of magnesium alloys should be lower than 0.5 mm/y to satisfy the requirement for BDS. According to recent research, Mg-based BDS should maintain mechanical support for 3–4 months to help the vessel remodeling [16], [52]. Therefore, for a BDS with a strut thickness of 150 μm, the degradation rate

should be lower than 0.23 mm/y. The *in-vitro* degradation rate of our Mg-Li stent was encouraging as it was as low as  $< 0.15$  mm/y ( $0.113 \pm 0.028$  mm/y before dilation and  $0.145 \pm 0.031$  mm/y after dilation, no statistical difference). The balloon dilation process did not make much difference to the degradation behaviors. Plastic deformation and residual stress resulted from the dilation process did not lead to deteriorated degradation, as depicted in Fig. 4. This is what we expected as the stent degraded uniformly, and avoided prematurely partial collapse.

However, the Mg-8.5Li stent has demonstrated swift degradation within 3 months in the iliac artery of minipigs. *In-vivo* degradation rate ( $> 0.6$  mm/y) of this stent was significantly higher than the *in-vitro* result ( $0.145 \pm 0.031$  mm/y). The fast *in-vivo* degradation profile was out of expectation. The disparity could be ascribed to the big differences between *in-vitro* and *in-vivo* environments (huge gaps in chemical, mechanical, fluidic, cellular and tissue aspects, etc.). Such rapid degradation may result in early recoil because of the lack of radial force exerted by the stent at this early stage of healing (showing insufficient mechanical support at 1 month). The short scaffolding duration is insufficient for coronary or peripheral applications, and needed to be improved in future work.

The radial strength (the strength at 10% compression of the original diameter) and radial stiffness (the strength to pro-

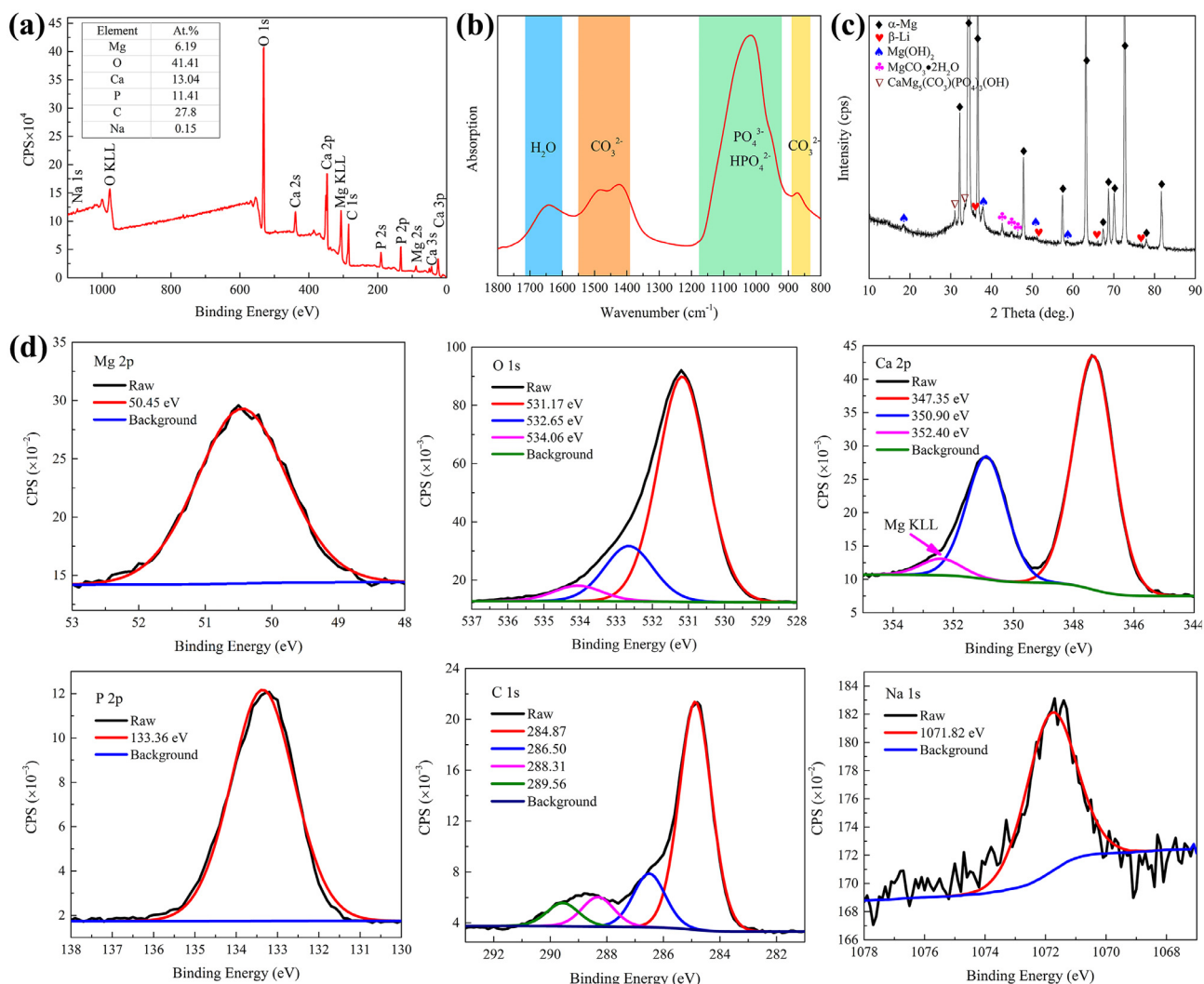


**Fig. 6.** (a) XPS spectrum, (b) FTIR spectrum, (c) XRD pattern, and (d) high resolution narrow XPS scanning results of the stent (after 7-day immersion in Hank's solution).

duce unit change in the stent diameter during radial compression) of the stent are measured to be  $59.5 \pm 4.6$  kPa, and  $166.79 \pm 34.06$  kPa/mm, respectively. Those values are lower than currently used DESs (non-biodegradable, a radial strength  $> 90$  kPa for current DESs) [53]. Insufficient radial force might result in lumen area loss after stent implantation. Poor mechanical properties of the Mg-8.5Li alloy matrix should be responsible for the low radial force, as Mg-8.5Li alloy exhibits a tensile strength of  $< 160$  MPa, while Magmaris Mg-alloy owns a tensile strength of 220–280 MPa. The radial force of present stent could be improved through optimizing the mechanical properties of the Mg-Li base alloy.

Nonetheless, the Mg-8.5Li stent still could be tolerated by surrounding tissues even under this intense degradation condition. In addition, only moderate tissue hyperplasia occurred, and that was not such bad, as already shown in Fig. 7. No calcification sites were found in the vessels through micro-CT examination (a spatial resolution of  $9 \mu\text{m}$ , particle size  $> 9 \mu\text{m}$  could be noticed) and histological analysis during the observation period. Basically, components and degradation products of the Mg-8.5Li stent were tolerable in iliac artery of minipigs. Tissue responses might be further improved if the degradation was well controlled.

Here, it should be emphasized that preclinical studies in animals so far have limitations to predict stent performance in human. Differences do exist in different species, and animal trials cannot fully reflect the stent performance in human body. The key parameters of a biodegradable stent may also be adjusted according to the clinical feedbacks, even if those items were perfectly verified in animal models. However, preclinical animal trials are indispensable during R&D process of implantable devices. So, it is very important and necessary to choose suitable animal models to simulate the in-human environment according to the specific test items and devices. For example, endothelialization rate is known to be faster in non-human animal models than in humans, and faster in pigs than in rabbits. So, rabbits may be more suitable for endothelialization evaluation of biodegradable stents [45]. For the general and preliminary safety and biocompatibility evaluations in this study, porcine artery is a proper and sufficient model.

#### 4.2. Comparison with other Mg-based BDSs

For in-depth understanding of the Mg-8.5Li stent performance, key performances (mainly focusing on the degradation behaviors and biocompatibility) of previously reported Mg-based BDSs were listed in Table 1 for comparison. A vast majority of those

**Table 1**  
*In-vitro* and *in-vivo* performances of previously reported Mg-based BDSs for intravascular applications.

Stent platform material	Strut thickness ( $\mu\text{m}$ )	Coating	<i>In-vitro</i> performance			<i>In-vivo</i> performance			Reference	
			Dilation	Degradation medium	Static/dynamic degradation	<i>In-vitro</i> degradation	Animal model	<i>In-vivo</i> degradation		<i>In-vivo</i> biocompatibility
AZ31B	150	NA	Yes	D-Hanks' solution, for 14 days	Static	Broken into separate pieces in 14 days (characterized by a stereo microscope)	NA	NA	NA	2013 [63]
AZ31	200	NA	Yes (from 4.5 mm to 6.3 mm)	DMEM+10% FBS+1% penicillin-streptomycin, in a bioreactor (5% CO <sub>2</sub> , 95% RH) for 7 days	Static	0.37 ± 0.07 mm/y (characterized by micro-CT)	NA	NA	NA	2014 [64]
AZ31	200	NA	Yes (from 4.5 mm to 6.3 mm)	DMEM+10% FBS+1% penicillin-streptomycin in a bioreactor (5% CO <sub>2</sub> , 95% RH) for 7 days	Dynamic (with a flow-induced shear stress of 0.05 Pa)	1.21 ± 0.27 mm/y (characterized by micro-CT)	NA	NA	NA	2014 [64]
AZ31	140	A fluoride chemical conversional coating	NA	Hank's solution without Mg and Ca	Static	45% weight loss after 28 days	NA	NA	NA	2019 [65]
AZ31	140	A fluoride chemical conversional coating + PDLLA coating	NA	Hank's solution without Mg and Ca	Static	< 10% weight loss after 28 days	NA	NA	NA	2019 [65]
AE21	150–200	NA	Yes (a stent/artery (diameter) ratio of 1.3)	NA	NA	NA	Pig coronary artery	Fully degraded in less than 90 days (characterized by measuring the strut cross-sectional area)	Significant narrowing (neointima formation) of lumen between days 10 and 35 caused by a short-period scaffolding	2003 [25]
AZ31B	155	A P(LA-TMC) coating containing sirolimus	Yes (a stent/artery (diameter) ratio of 1.1–1.3)	NA	NA	NA	Rabbit infrarenal abdominal aorta	Full degradation in 6 months (characterized by measuring strut sectional area)	Reduced neointimal area, but delayed endothelialization compared to uncoated stent	2011 [26]
AZ91	80–120	NA	Yes	NA	NA	NA	Coronary/femoral artery of dogs	Completely disappeared after 7 days (characterized by X-ray)	No thrombosis, and moderate intimal hyperplasia was found after 14 days	2015 [27]
AZ31B	140	A fluoride chemical conversional coating + PDLLA coating	Yes (a stent/artery (diameter) ratio of 1.1–1.2)	NA	NA	NA	Porcine coronary artery	More than 50% struts fractured (at the maximum stress site) after 1 month (characterized by X-ray tomography)	Completely embraced by neointima after 1 month and a slightly thicker intima, good blood compatibility and histocompatibility	2020 [72]
Mg-2.0Zn-0.5Y-0.5Nd	150–180	A APTES silane physical barrier layer + rapamycin-eluting PLGA coating	Yes (a stent/artery (diameter) ratio of 1.0–1.1)	NA	NA	NA	Porcine coronary artery	Stent strut mainly remained after 3 months, only limited strut residues was found after 6 months (characterized through histology)	Benign tissue compatibility as well as re-endothelialization without thrombogenesis or in-stent restenosis during 6-month followup	2016 [66]
Mg-2.5Nd-0.21Zn-0.44Zr (JDBM)	150	NA	Yes	NA	NA	NA	Rabbit abdominal artery	Without the tube wall fractured after 4 months (characterized by micro-CT)	Good biocompatibility	2017 [67]

(continued on next page)

Table 1 (continued)

Stent platform material	Strut thickness ( $\mu\text{m}$ )	Coating	<i>In-vitro</i> performance			<i>In-vitro</i> degradation	<i>In-vivo</i> performance	<i>In-vivo</i> degradation	<i>In-vivo</i> biocompatibility	Reference
			Dilation	Degradation medium	Static/dynamic degradation					
Mg-2.1Nd-0.21Zn-0.5Zr (JDBM)	150	NA	Yes ((a stent/artery (diameter) ratio of 1.1–1.2)	NA	NA	NA	Rabbit common carotid artery	Some stent strut fractures after 1 month, stent struts broke into pieces after 4 months (characterized by micro-CT)	Good safety and efficacy with a complete re-endothelialization within 28 days, low risks of possible vessel calcification	2018 [73]
Mg-2.1Nd-0.21Zn-0.5Zr (JDBM)	150	A bare stent (covered by an expandable e-PTFE membrane)	Yes	NA	NA	NA	Rabbit common carotid artery (a lateral aneurysm model)	Integrated stent structure was found after 2 weeks. The contour of the stent became vague after 6 months, and could not be visualized after 1 year (characterized by molybdenum target examination)	Disappearance of the aneurysms and patency of the carotid artery. The covered stents proved to be an effective approach for occlusion of lateral aneurysm in the rabbit common carotid artery	2016 [68]
Mg-2.5Nd-0.2Zn-0.4Zr (JDBM)	150	A protective MgF <sub>2</sub> layer + PDLLA coating containing sirolimus	Yes (a stent/artery (diameter) ratio of 1.1)	NA	NA	NA	Porcine coronary artery	A remarkably lower degradation rate compared to bare stent, integral structure with only occasional fractures after 2 months (characterized by micro-CT)	Favorable safety with no occurrence of adverse complications, similar neointima proliferation compared to a commercial Firebird 2 DES	2017 [74]
Mg-2.1Nd-0.2Zn-0.5Zr (JDBM)	150	A protective MgF <sub>2</sub> layer + PLT base coating and PLGA top coating containing sirolimus	Yes	NA	NA	NA	Rabbit iliac artery	A volume loss of 64% after 5 months (characterized by micro-CT)	No thrombus or early restenosis, suitable biocompatibility	2019 [62]
AMS, Biotronik (WE43)	165	NA	Yes	NA	NA	NA	Porcine coronary artery	Degraded over a 3-month time period (characterized by OCT and histology)	A progressive degradation of the stents, no significant increase in neointimal area.	2008 [69]
AMS, Biotronik (WE43)	165	NA	Yes	NA	NA	NA	Human coronary artery	Nearly complete degradation at 4 months (characterized by IVUS)	Early recoil as a main contributor for restenosis at 4 months	2009 [57]
DREAMS-1 G120 Biotronik (WE43)	120	A PLGA coating with paclitaxel	Yes	NA	NA	NA	Human coronary artery	Resorption time was within 6 months (characterized by OCT and IVUS)	A faster than expected stent degradation with an early loss of radial force and consequent vessel recoil.	2013 [70]
DREAMS-2 G/Magmaris, Biotronik (WE43)	150	A PLLA coating with sirolimus	Yes	NA	NA	NA	Human coronary artery	Scaffolding time up to 3 months and the resorption time prolonged to 12 months (characterized by OCT and IVUS)	Clinical evidence of safety and efficacy [20],[71]	2016–2020 [20],[71]
Mg-0.3Sr-0.3Ca <sup>#</sup>	250	NA	Yes	NA	NA	NA	Femoral artery of Beagle dog	The wall thickness decreased from 250 $\mu\text{m}$ to ~200 $\mu\text{m}$ after 5 weeks (characterized by histology)	No sign of occlusion, no thrombosis, in situ formation of Sr-substituted HA on the stent surface	2016 55

(continued on next page)

Table 1 (continued)

Stent platform material	Strut thickness ( $\mu\text{m}$ )	Coating	<i>In-vitro</i> performance			<i>In-vitro</i> degradation	<i>In-vivo</i> performance	<i>In-vivo</i> degradation	<i>In-vivo</i> biocompatibility	Reference
			Dilation	Degradation medium	Static/dynamic degradation					
WE43	250	NA	Yes	NA	NA	NA	Femoral artery of Beagle dog	The wall thickness did not change significantly after 5 weeks (characterized by histology)	Artery was extensively occluded and thrombosed. Suspected to be related to rare-earth elements	2016 55
Mg-8.5Li#	150	NA	Yes (a stent/artery (diameter) ratio of 1.06–1.17)	Hank's solution at $37 \pm 0.5^\circ\text{C}$ for 7 days	Static	$0.145 \pm 0.03 \text{ mm}^2/\text{y}$ (characterized by weight loss)	Porcine iliac artery	Degradation rate > 0.6 mm/y, scaffolding time less than 1 month, almost fully degraded in 3 months	No possible thrombus, endothelial coverage in 1-month, acceptable histocompatibility	Present work

PDLLA: poly(D,L-lactide), P(LA-TMC): poly(lactic acid-co-trimethylene carbonate), APTES: cross-linked 3-amino-propyltrimethoxysilane, PLGA: poly lactic-co-glycolic acid, PTFE: polytetrafluoroethylene, PLT: poly (l-lactide-co-trimethylene carbonate), PLLA: poly-L-lactide. #: rare earth-free and aluminum-free.

BDSs were fabricated from the AZ-based (Al-containing) or RE-containing alloy series. Except for one WE43 stent, which was reported to be associated with occluded and thrombosed artery (suspected to be related to rare-earth elements) according to the research of Bornapour et al. , the remaining Mg-based BDSs exhibited proper or good biocompatibility. The strut thickness of currently developed Mg-based BDSs was in the range of 80–250  $\mu\text{m}$ , usually to be 150  $\mu\text{m}$ . *In-vitro* degradation rate of our Mg-8.5Li stent was smaller than that of other bare Mg-based BDSs, and the *in-vivo* degradation rate was comparable to its counterparts without coat-

ings. Apparently, Mg-Li based BDS shows virtue from the criteria of elemental biocompatibility.

### 4.3. Perspectives on future development of Mg-Li alloy based BDS

#### 4.3.1. Stronger platform material and thinner stent strut

The strut thickness is a crucial parameter for both permanent stents and biodegradable stents, as it is associated with local flow pattern and endothelialization, which have been shown to influence local inflammation, rate of restenosis, and thrombogenicity [54]. Thinner strut leads to better clinical performances

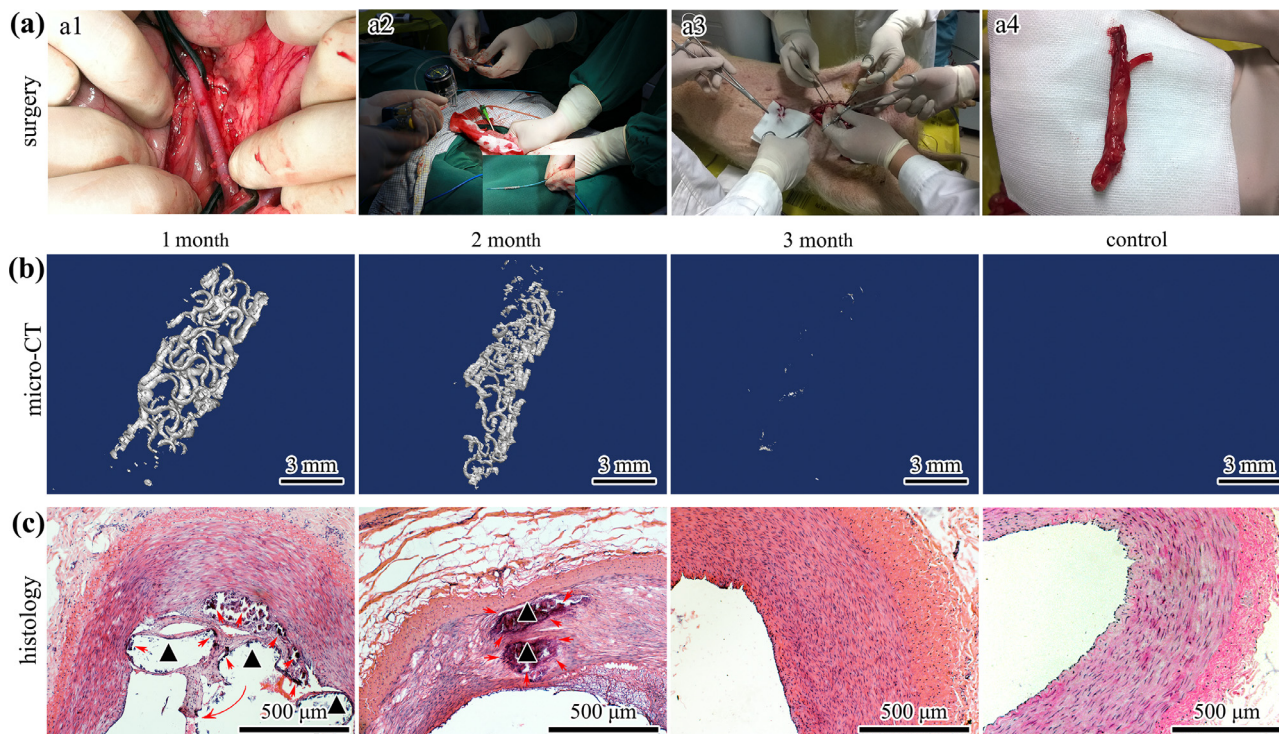
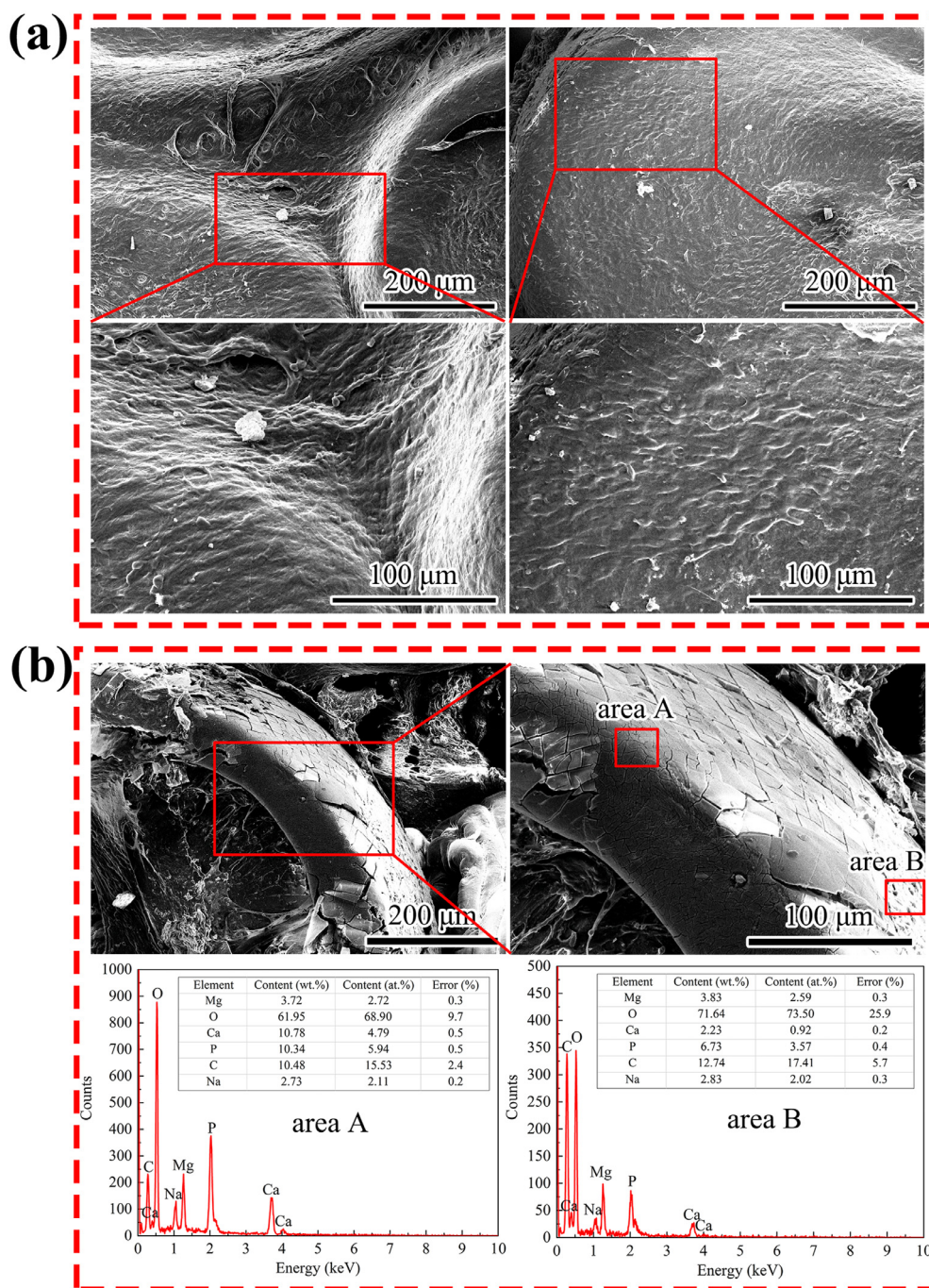


Fig. 7. (a) The implantation surgery and retrieval of stented vessels (a1: exposure of the iliac artery, a2: stent deployment process, a3: laparotomy during sample retrieval, a4: the retrieved iliac artery), (b) 3D reconstruction of the remaining stent from micro-CT analysis, (c) typical histological images of the stented iliac arteries at different time points, with normal iliac artery as control. Black triangles indicate the positions of the stent struts, and possible absence of the struts was caused by the slicing process or H&E staining procedure. Red arrows indicate the presence of debris or degradation products. The long red arrow shows some of the tissues surrounding the struts were torn away from their original positions during slicing procedure. (For interpretation of the references to colour in this figure legend, the reader is referred to the web version of this article.)



**Fig. 8.** (a) The status of endothelial coverage on Mg-8.5Li alloy stent after 1 month in iliac artery of minipigs characterized by SEM (typical areas on the strut and in the intermediate spaces of the struts were displayed, tiny particles were salt deposits derived from the tissue fixation and dehydration process.), (b) typical *in-vivo* corrosion morphology of the stent and corresponding EDS analysis at regions of interest.

as proved through the evolution of DESs [55,56]. However, current Mg-based stents own thicker struts compared to the prevailing DESs, as shown in Table 1. In addition, thicker strut is a common problem faced by all kinds of biodegradable stents (whether polymeric or metallic stents) at this stage [45]. There are 5 CE marked biodegradable stents on market, including ART (164 μm, 2015), Magmaris (170 μm, 2016), Fantom (125 μm, 2017), DESolve Cx (120 μm, 2017), and MeRes100 (100 μm, 2019). Strut thicknesses (with coating) of ART and Magmaris are both higher than 150 μm.

Thin-strut design is the future development trend of biodegradable stents. The next generation (DREAMS 3 G) of Magmaris (also known as DREAMS 2 G, a strut thickness of 150 μm) is being developed with thinner strut thickness (99–150 μm) and prolonged scaffolding time. A robust platform material favors for the design of thinner strut, without compensation of radial strength. Alloying with Li provides with desirable ductility, the basis for balloon expandable BDS. However, the strength of binary Mg-Li alloys is generally less than satisfactory (resulting in a lower radial strength of Mg-8.5Li alloy stent compared to current DESs). Another supple-

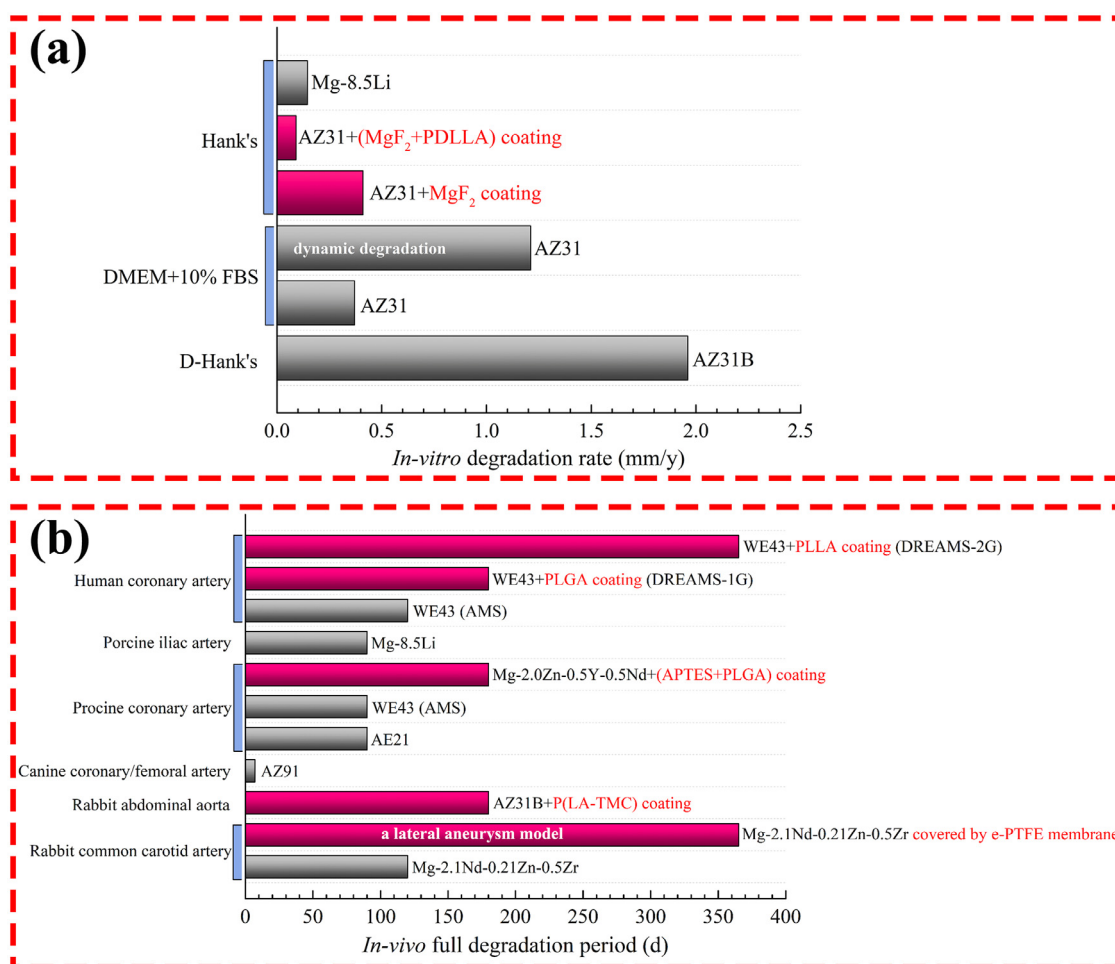


**Fig. 9.** (a) *In-vitro* degradation rates of previously reported Mg-based BDSs (with or without coating, the columns of stents with coatings were in magenta) in different mediums, data were from Refs [63–65]. (b) the *in-vivo* degradation periods of various Mg-based BDSs in different animal models, data were collected from Refs[25–27],[57],[66,67,70,70].

mentary alloying element can be helpful in enhancing mechanical strength, and Zn might be a proper choice herein [41].

#### 4.3.2. Deal with the fast degradation of Mg-Li BDS

Fig. 9 compared the *in-vitro* degradation rates and *in-vivo* full degradation periods of various Mg-based BDSs with or without protective coatings. Generally, excessive degradation is a prevalent problem faced by bare Mg-based BDSs, and the degradation duration ranges from several days to a few months among different BDS platform materials [6,27,57]. Surface coating is an effective way which can substantially improve corrosion resistance [58]. It helps maintain the mechanical integrity for a longer time, and improves Mg-based BDS performance. Even for the precursor of Magmaris, i.e. the first generation of absorbable metallic stent AMS in Biotronik, the durability was only 3–4 months in porcine coronaries or in human coronary arteries [57,59]. Polymeric coating was adopted on the next two generations (DREAMS 1 G and DREAM 2 G), along with refined platform material, the scaffolding time was prolonged to 3 months, and the whole degradation period was improved up to 12 months [20]. The clinical experience with DESs by using limus-type (sirolimus, everolimus) anti-proliferative drugs to lower hyperplasia should also be considered in R&D of Mg-based BDSs.

As we mentioned before, dilation/expansion of Mg-based BDSs is through plastic deformation. The maximum strain during stent deployment should not exceed the fracture limit of the platform

material. A certain extent of plastic deformation and residual stress have been shown to affect the degradation behavior [60,61]. The maximum strain and maximum residual stress induced during the deployment process should be strictly controlled. Otherwise, severely localized degradation could happen at those sites, leading to non-uniform degradation and premature fracture. Proper pattern design and shape optimization through FEA method is practicable in improving the performance of Mg-based BDSs [62].

#### 4.4. Limitations in this study

It should be noted that this study has examined only the preliminary feasibility of a novel BDS based on a binary Mg-Li alloy free of Al and RE. We only concentrated on the degradation behaviors and general biocompatibility of this stent. There are shortcomings on stent performances at this stage, but there are ways to improve. Sufficient radial strength at a thinner strut level and prolonged degradation period are the goals of our next generation Mg-Li alloy-based stent. Further evaluations, including lumen area (restenosis) and endothelial function, are important for a finished stent product, and those items will be covered in our future work on a more reliable Mg-Li alloy-based stent. Differences between species should not be ignored. The healthy pig artery model could not fully reflect the real stenosed human artery. The endothelialization process and thrombus risk may be different in human artery.

## 5. Conclusions

In the present study, the feasibility of a novel Mg-8.5Li stent to be used in the treatment of stenosed vessels was preliminarily evaluated, mainly focusing on the degradation behaviors and *in-vivo* biocompatibility. Plastic deformation and residual stress derived from the balloon dilation process did not lead to deteriorated degradation. This stent exhibited a decent degradation rate of < 0.15 mm/y *in vitro*, showing possibility to maintain for a long scaffolding period *in vivo*. However, its implantation in iliac artery of minipigs revealed divergent results (degradation rate > 0.6 mm/y), showing an insufficient scaffolding time. The basic thing, though, is that this stent did not induce possible thrombus, and it was tolerable in surrounding arterial tissues. Besides, endothelial coverage of the stent was achieved within 1 month even under this radical degradation condition. The radial strength and degradation profile need to be well controlled to improve *in-vivo* performance in future work.

## Declaration of Competing Interest

The authors declare that they have no known competing financial interests or personal relationships that could have appeared to influence the work reported in this paper.

## Acknowledgements

This work was supported by the National Key R&D Program of China (2016YFC1102400), National Natural Science Foundation of China (Grant No. 51871004), and NSFC/RGC Joint Research Scheme (Grant No. 51661165014).

## References

- [1] R.L. Mueller, T.A. Sanborn, The history of interventional cardiology: cardiac catheterization, angioplasty, and related interventions, *Am. Heart J.* 129 (1) (1995) 146–172.
- [2] U. Sigwart, J. Puel, V. Mirkovitch, F. Joffre, L. Kappenberger, Intravascular stents to prevent occlusion and restenosis after transluminal angioplasty, *N. Engl. J. Med.* 316 (12) (1987) 701–706.
- [3] J. Iqbal, J. Gunn, P.W. Serruys, Coronary stents: historical development, current status and future directions, *Brit. Med. Bull.* 106 (1) (2013) 193–211.
- [4] P.W. Serruys, M.J.B. Kutryk, A.T.L. Ong, Coronary-artery stents, *N. Engl. J. Med.* 354 (5) (2006) 483–495.
- [5] A. Purnama, H. Hermawan, D. Mantovani, Biodegradable metal stents: a focused review on materials and clinical studies, *J. Biomater. Tiss. Eng.* 4 (11) (2014) 868–874.
- [6] Y.Q. Zhu, K. Yang, R.Y. Cheng, Y. Xiang, T.W. Yuan, Y.S. Cheng, B. Sarmento, W.G. Cui, The current status of biodegradable stent to treat benign luminal disease, *Mater. Today* 20 (9) (2017) 516–529.
- [7] H.S. Han, S. Loffredo, I. Jun, J. Edwards, Y.C. Kim, H.K. Seok, F. Witte, D. Mantovani, S. Glyn-Jones, Current status and outlook on the clinical translation of biodegradable metals, *Mater. Today* 23 (2019) 57–71.
- [8] N. Kukreja, Y. Onuma, J. Daemen, P.W. Serruys, The future of drug-eluting stents, *Pharmacol. Res.* 57 (3) (2008) 171–180.
- [9] M.J. Eisenberg, K.J. Konnyu, Review of randomized clinical trials of drug-eluting stents for the prevention of in-stent restenosis, *Am. J. Cardiol.* 98 (3) (2006) 375–382.
- [10] A.T.L. Ong, E.P. Mcfadden, E. Regar, P.P.T.D. Jaegers, R.T.V. Domburg, P.W. Serruys, Late angiographic stent thrombosis (LAST) events with drug-eluting stents, *J. Am. Coll. Cardiol.* 45 (12) (2005) 2088–2092.
- [11] A.A. Bavry, D.L. Bhatt, Appropriate use of drug-eluting stents: balancing the reduction in restenosis with the concern of late thrombosis, *Lancet* 371 (9630) (2008) 2134–2143.
- [12] S.H. Hofma, V.D.G. Wj, B.M. van Dalen, P.A. Lemos, E.P. Mcfadden, G. Sianos, J.M. Ligthart, E.D. Van, P.J. de Feyter, P.W. Serruys, Indication of long-term endothelial dysfunction after sirolimus-eluting stent implantation, *Eur. Heart J.* 27 (2) (2006) 166–170.
- [13] M. Togni, S. Windecker, R. Cocchia, P. Wenaweser, S. Cook, M. Billinger, B. Meier, O.M. Hess, Sirolimus-eluting stents associated with paradoxical coronary vasoconstriction, *J. Am. Coll. Cardiol.* 46 (2) (2005) 231–236.
- [14] A.V. Finn, M. Joner, G. Nakazawa, F. Kolodgie, J. Newell, M.C. John, H.K. Gold, R. Virmani, Pathological correlates of late drug-eluting stent thrombosis: strut coverage as a marker of endothelialization, *Circulation* 115 (18) (2007) 2435–2441.
- [15] G. Mani, M.D. Feldman, D. Patel, C.M. Agrawal, Coronary stents: a materials perspective, *Biomaterials* 28 (9) (2007) 1689–1710.
- [16] Y.F. Zheng, X.N. Gu, F. Witte, Biodegradable metals, *Mat. Sci. Eng. R.* 77 (0) (2014) 1–34.
- [17] M. Haude, H. Ince, A. Abizaid, R. Toelg, P.A. Lemos, C. von Birgelen, E.H. Christiansen, W. Wijns, F.J. Neumann, C. Kaiser, E. Eeckhout, S.T. Lim, J. Escaned, H.M. Garcia-Garcia, R. Waksman, Safety and performance of the second-generation drug-eluting absorbable metal scaffold in patients with de-novo coronary artery lesions (BIOSOLVE-II): 6 month results of a prospective, multicentre, non-randomised, first-in-man trial, *Lancet* 387 (10013) (2016) 31–39.
- [18] <http://www.magmaris.com/>, last accessed on September 17, 2020.
- [19] H. Hermawan, D. Dubé, D. Mantovani, Developments in metallic biodegradable stents, *Acta Biomater* 6 (5) (2010) 1693–1697.
- [20] J. Bennett, Q.D. Hemptinne, K. McCutcheon, Magmaris resorbable magnesium scaffold for the treatment of coronary heart disease: overview of its safety and efficacy, *Expert Rev. Med. Devic.* 16 (9) (2019) 757–769.
- [21] J. Vormann, Magnesium: nutrition and metabolism, *Mol. Aspects of Med.* 24 (1–3) (2003) 27–37.
- [22] F. Witte, Reprint of: the history of biodegradable magnesium implants: a review, *Acta Biomater* 23 (2015) S28–S40.
- [23] Y. Onuma, T. Muramatsu, A. Kharlamov, P.W. Serruys, Freeing the vessel from metallic cage: what can we achieve with bioresorbable vascular scaffolds? *Cardiovasc. Interv. Ther.* 27 (3) (2012) 141–154.
- [24] R. Waksman, R. Pakala, P.K. Kuchulakanti, R. Baffour, D. Hellings, R. Seabron, F.O. Tio, E. Wittchow, S. Hartwig, C. Harder, R. Rohde, B. Heublein, A. Andreae, K.-H. Waldmann, A. Haverich, Safety and efficacy of bioabsorbable magnesium alloy stents in porcine coronary arteries, *Catheter. Cardio. Inte.* 68 (4) (2006) 607–617.
- [25] B. Heublein, R. Rohde, V. Kaese, N. Niemeyer, W. Hartung, A. Haverich, Biocorrosion of magnesium alloys: a new principle in cardiovascular implant technology? *Heart* 89 (6) (2003) 651–656.
- [26] H.W. Li, H.S. Zhong, K. Xu, K. Yang, J. Liu, B.C. Zhang, F. Zheng, Y.H. Xia, L.L. Tan, D. Hong, Enhanced efficacy of sirolimus-eluting bioabsorbable magnesium alloy stents in the prevention of restenosis, *J. Endovasc. Ther.* 18 (3) (2011) 407–415.
- [27] Y. Yue, L.L. Wang, N. Yang, J.L. Huang, L.C. Lei, H.M. Ye, L.H. Ren, S.X. Yang, Effectiveness of biodegradable magnesium alloy stents in coronary artery and femoral artery, *J. Interv. Cardiol.* 28 (4) (2015) 358–364.
- [28] Y.J. Shi, L. Zhang, J.H. Chen, J. Zhang, F. Yuan, L. Shen, C.X. Chen, J. Pei, Z.H. Li, J.Y. Tan, G.Y. Yuan, In vitro and in vivo degradation of rapamycin-eluting Mg-Nd-Zn-Zr alloy stents in porcine coronary arteries, *Mat. Sci. Eng. C.* 80 (2017) 1–6.
- [29] P.C. Ferreira, K.A. Piai, A.M. Takayanagui, S.I. Segura-Muñoz, Aluminum as a risk factor for Alzheimer's disease, *Rev. Latino-Am. Enfermagem* 16 (1) (2008) 151–157.
- [30] F. Feyerabend, J. Fischer, J. Holtz, F. Witte, R. Willumeit, H. Drücker, C. Vogt, N. Hort, Evaluation of short-term effects of rare earth and other elements used in magnesium alloys on primary cells and cell lines, *Acta Biomater* 6 (5) (2010) 1834–1842.
- [31] A. Drynda, N. Deinet, N. Braun, M. Peuster, Rare earth metals used in biodegradable magnesium-based stents do not interfere with proliferation of smooth muscle cells but do induce the upregulation of inflammatory genes, *J. Biomed. Mater. Res. A.* 91A (2) (2009) 360–369.
- [32] D. Szklarska, P. Rzymiski, Is lithium a micronutrient? from biological activity and epidemiological observation to food fortification, *Biol. Trace Elem. Res.* 189 (2019) 18–27.
- [33] M. Gitlin, Lithium side effects and toxicity: prevalence and management strategies, *Int. J. of Bipolar Disord.* 4 (2016) 27.
- [34] A.M. Pérez-Granados, M.P. Vaquero, Silicon, aluminium, arsenic and lithium: essentiality and human health implications, *J. Nutr. Health Aging* 6 (2) (2002) 154–162.
- [35] M. Qassem, L. Constantinou, I.F. Triantis, M. Hickey, E. Palazidou, P.A. Kyriacou, A method for rapid, reliable, and low-volume measurement of lithium in blood for use in bipolar disorder treatment management, *IEEE T. Bio-med. Eng.* 66 (1) (2019) 130–137.
- [36] B. Bosche, M. Molcanyi, S. Rej, T.R. Doepfner, M. Obermann, D.J. Müller, A. Das, J. Hescheler, R.L. Macdonald, T. Noll, F.V. Härtel, Low-dose lithium stabilizes human endothelial barrier by decreasing MLC phosphorylation and universally augments cholinergic vasorelaxation capacity in a direct manner, *Front. Physiol.* 7 (593) (2016), doi:10.3389/fphys.2016.00593.
- [37] F.W. Bach, M. Schaper, C. Jaschik, Influence of lithium on hcp magnesium alloys, *Mater. Sci. Forum.* 419–422 (2003) 1037–1042.
- [38] F. Witte, J. Fischer, J. Nellesen, C. Vogt, J. Vogt, T. Donath, F. Beckmann, In vivo corrosion and corrosion protection of magnesium alloy LAE442, *Acta Biomater* 6 (5) (2010) 1792–1799.
- [39] D.D. Xia, Y. Liu, S.Y. Wang, R.C. Zeng, Y.S. Liu, Y.F. Zheng, Y.S. Zhou, In vitro and in vivo investigation on biodegradable Mg-Li-(Al) alloys for bone implant application, *Sci. China Mater.* 62 (2) (2019) 256–272.
- [40] W.R. Zhou, Y.F. Zheng, M.A. Leeftang, J. Zhou, Mechanical property, biocorrosion and in vitro biocompatibility evaluations of Mg-Li-(Al)-(RE) alloys for future cardiovascular stent application, *Acta Biomater* 9 (10) (2013) 8488–8498.
- [41] Y. Liu, Y.H. Wu, D. Bian, S. Gao, S. Leeftang, H. Guo, Y.F. Zheng, J. Zhou, Study on the Mg-Li-Zn ternary alloy system with improved mechanical properties, good degradation performance and different responses to cells, *Acta Biomater* 62 (2017) 418–433.
- [42] ASTM G31-72Standard Practice for Laboratory Immersion Corrosion Testing of Metals, ASTM International, West Conshohocken, PA, 2004 2004.

- [43] ASTM G1-03 Standard Practice for Preparing, Cleaning, and Evaluating Corrosion Test Specimens e1, ASTM International, West Conshohocken, PA, 2017 2017.
- [44] Z.M. Shi, M. Liu, A. Atrens, Measurement of the corrosion rate of magnesium alloys using Tafel extrapolation, *Corros. Sci.* 52 (2) (2010) 579–588.
- [45] W.J. Lin, H.J. Zhang, W.Q. Zhang, H.P. Qi, G. Zhang, J. Qian, X. Li, L. Qin, H.F. Li, X. Wang, H. Qiu, X.L. Shi, W. Zheng, D.Y. Zhang, R.L. Gao, J.D. Ding, In vivo degradation and endothelialization of an iron bioresorbable scaffold, *Bioact. Mater.* 6 (4) (2021) 1028–1039.
- [46] T. Fu, J.T. Fan, Y.G. Shen, J.M. Sun, Hydrothermal calcification of alkali treated titanium in CaHPO<sub>4</sub> solution, *Mater. Chem. Phys.* 189 (2017) 105–110.
- [47] B. Demri, D. Muster, XPS study of some calcium compounds, *J. Mater. Process. Technol.* 55 (3–4) (1995) 311–314.
- [48] H.R. Bakhsheshi-Rad, M.H. Idris, M.R. Abdul-Kadir, A. Ourdjini, M. Medraj, M. Daroonparvar, E. Hamzah, Mechanical and bio-corrosion properties of quaternary Mg–Ca–Mn–Zn alloys compared with binary Mg–Ca alloys, *Mater. Design* 53 (2014) 283–292.
- [49] P.K. Bowen, J. Drelich, J. Goldman, Magnesium in the murine artery: probing the products of corrosion, *Acta Biomater.* 10 (3) (2014) 1475–1483.
- [50] M. Bauer, M. Gitlin, *The Essential Guide to Lithium Treatment*, Springer International Publishing, 2016.
- [51] M. Erinc, W.H. Sillekens, R.G.T.M. Mannens, R.J. Werkhoven, Applicability of existing magnesium alloys as biomedical implant materials, *Magnesium Technol.* (2009) 209–214.
- [52] Y. Onuma, P.W.J.C. Serruys, *Bioresorbable Scaffolds: From Basic Concept to Clinical Applications*, CRC Press, 2017.
- [53] W.J. Lin, L. Qin, H.P. Qi, D.Y. Zhang, G. Zhang, R.L. Gao, H. Qiu, Y. Xia, P. Cao, X. Wang, W. Zheng, Long-term in vivo corrosion behavior, biocompatibility and bioresorption mechanism of a bioresorbable nitrided iron scaffold, *Acta Biomater.* 54 (2017) 454–468.
- [54] M. Bornapour, H. Mahjoubi, H. Vali, D. Shum-Tim, M. Cerruti, M. Pegguleryuz, Surface characterization, in vitro and in vivo biocompatibility of Mg-0.3Sr-0.3Ca for temporary cardiovascular implant, *Mater. Sci. Eng. C* 67 (2016) 72–84.
- [55] H. Jinnouchi, S. Torii, A. Sakamoto, F.D. Kolodgie, R. Virmani, A.V. Finn, Fully bioresorbable vascular scaffolds: lessons learned and future directions, *Nat. Rev. Cardiol.* 16 (5) (2019) 286–304.
- [56] A. Lupi, A. Schaffer, A.S. Bongo, Should ultrathin strut drug eluting stents be considered the new benchmark for novel coronary stents approval? The complex interplay between stent strut thickness, polymeric carriers and antiproliferative drugs, *J. Thorac. Dis.* 10 (2) (2018) 678–681.
- [57] C. Indolfi, S.D. Rosa, A. Colombo, Bioresorbable vascular scaffolds - basic concepts and clinical outcome, *Nat. Rev. Cardiol.* 13 (12) (2016) 719–729.
- [58] R. Waksman, R. Erbel, C. Di Mario, J. Bartunek, B. de Bruyne, F.R. Eberli, P. Erne, M. Haude, M. Horrigan, C. Ilesley, D. Böse, H. Bonnier, J. Koolen, T.F. Lüscher, N.J. Weissman, Early- and long-term intravascular ultrasound and angiographic findings after bioabsorbable magnesium stent implantation in human coronary arteries, *JACC: Cardiovasc. Int.* 2 (4) (2009) 312–320.
- [59] M. Echeverry-Rendon, J.P. Allain, S.M. Robledo, F. Echeverria, M.C. Harmsen, Coatings for biodegradable magnesium-based supports for therapy of vascular disease: a general view, *Mater. Sci. Eng. C* 102 (2019) 150–163.
- [60] T.L. Pinto Slottow, R. Pakala, R. Waksman, Serial imaging and histology illustrating the degradation of a bioabsorbable magnesium stent in a porcine coronary artery, *Eur. Heart J.* 29 (3) (2008) 314.
- [61] E. Galvin, C. Cummins, S. Yoshihara, B.J. Mac Donald, C. Lally, Plastic strains during stent deployment have a critical influence on the rate of corrosion in absorbable magnesium stents, *Med. Biol. Eng. Comput.* 55 (8) (2017) 1261–1275.
- [62] Y.M. Gao, L.Z. Wang, L.H. Li, X.N. Gu, K. Zhang, J. Xia, Y.B. Fan, Effect of stress on corrosion of high-purity magnesium in vitro and in vivo, *Acta Biomater* 83 (2019) 477–486.
- [63] C.X. Chen, J.H. Chen, W. Wu, Y.J. Shi, L. Jin, L. Petrini, L. Shen, G.Y. Yuan, W.J. Ding, J.B. Ge, E.R. Edelman, F. Migliavacca, In vivo and in vitro evaluation of a biodegradable magnesium vascular stent designed by shape optimization strategy, *Biomaterials* 221 (2019) 119414.
- [64] W. Wu, S.S. Chen, D. Gastaldi, L. Petrini, D. Mantovani, K. Yang, L.L. Tan, F. Migliavacca, Experimental data confirm numerical modeling of the degradation process of magnesium alloys stents, *Acta Biomater.* 9 (10) (2013) 8730–8739.
- [65] J. Wang, V. Giridharan, V. Shanov, Z.G. Xu, B. Collins, L. White, Y. Jang, J. Sankar, N. Huang, Y. Yun, Flow-induced corrosion behavior of absorbable magnesium-based stents, *Acta Biomater.* 10 (12) (2014) 5213–5223.
- [66] S.S. Chen, P. Wan, B.C. Zhang, D. Eren Erişen, H. Yang, K. Yang, A novel polymer critical re-melting treatment for improving corrosion resistance of magnesium alloy stent, *J. Mater. Sci. Technol.* 35 (1) (2019) 19–22.
- [67] J. Liu, B. Zheng, P. Wang, X.G. Wang, B. Zhang, Q.P. Shi, T.F. Xi, M. Chen, S.K. Guan, Enhanced in vitro and in vivo performance of Mg-Zn-Y-Nd alloy achieved with APTES pre-treatment for drug-eluting vascular stent application, *ACS Appl. Mater. Interf.* 8 (2016) 17842–17858.
- [68] L. Mao, H. Zhou, L. Chen, J.L. Niu, L. Zhang, G.Y. Yuan, C.L. Song, Enhanced biocompatibility and long-term durability in vivo of Mg-Nd-Zn-Zr alloy for vascular stent application, *J. Alloy. Compd.* 720 (2017) 245–253.
- [69] W. Wang, Y.L. W, M. Chen, L. Chen, J. Zhang, Y.D. Li, M.H. Li, G.Y. Yuan, Magnesium alloy covered stent for treatment of a lateral aneurysm model in rabbit common carotid artery: an in vivo study, *Sci. Rep.* 6 (2016) 37401.
- [70] T.L. Pinto Slottow, R. Pakala, T. Okabe, D. Hellinga, R.J. Lovelace, F.O. Tio, A.B. Bui, R. Waksman, Optical coherence tomography and intravascular ultrasound imaging of bioabsorbable magnesium stent degradation in porcine coronary arteries, *Cardiovasc. Revasc. Med.* 9 (4) (2008) 248–254.
- [71] M. Haude, R. Erbel, P. Erne, S. Verheyne, H. Degen, D. Böse, P. Vermeersch, I. Wijnbergen, N. Weissman, F. Prati, R. Waksman, J. Koolen, Safety and performance of the drug-eluting absorbable metal scaffold (DREAMS) in patients with de-novo coronary lesions: 12 month results of the prospective, multicentre, first-in-man BIOSOLVE-I trial, *Lancet* 381 (9869) (2013) 836–844.
- [72] Y. Ozaki, H.M. Garcia-Garcia, E. Shlofmitz, A. Hideo-Kajita, R. Waksman, Second-generation drug-eluting resorbable magnesium scaffold: review of the clinical evidence, *Cardiovasc. Revasc. Med.* 21 (1) (2020) 127–136.
- [73] S.S. Chen, B. Zhang, B.C. Zhang, H. Lin, H. Yang, F. Zheng, M. Chen, K. Yang, Assessment of structure integrity, corrosion behavior and microstructure change of AZ31B stent in porcine coronary arteries, *J. Mater. Sci. Technol.* 39 (2020) 39–47.
- [74] J. Zhang, H.Y. Li, W. Wang, H. Huang, J. Pei, H.Y. Qu, G.Y. Yuan, Y.D. Li, The degradation and transport mechanism of a Mg-Nd-Zn-Zr stent in rabbit common carotid artery: a 20-month study, *Acta Biomater.* 69 (2018) 372–384.
- [75] Y.J. Shi, L. Zhang, J.H. Chen, J. Zhang, F. Yuan, L. Shen, C.X. Chen, J. Pei, Z.H. Li, J.Y. Tan, G.Y. Yuan, In vitro and in vivo degradation of rapamycin-eluting Mg-Nd-Zn-Zr alloy stents in porcine coronary arteries, *Mater. Sci. Eng. C* 80 (2017) 1–6.